Elastic modulus changes in cementitious materials submitted to thermal treatments up to 1000°C

Sylvie Masse, G. Vetter, F. Boch, C. Haehnel

Elastic modulus changes in cementitious materials submitted to thermal treatments up to 1000°C

S. Masse,* G. Vetter,* P. Boch* and C. Haehnel†

Ecole Supérieure de Physique et de Chimie Industrielles; Association Technique de l'Industrie des Liants Hydrauliques

Three categories of cementitious materials (Portland cement pastes, siliceous and calcareous sand mortars, and microconcretes with siliceous sand and silica fume) were subjected to cumulative thermal treatments at temperatures (T) up to 1000°C. Changes in room-temperature elastic modulus $E^*(T)$ of heat treated materials was followed by a non-destructive ultrasonic technique at 10 MHz. Each category exhibits specific changes in $E^*(T)/E^*_0$ vs. T, where E^*_0 was the value before heat treatment, irrespective to the water:binder ratio.

Introduction

Accidental fires expose concrete structures to high temperatures. In Europe, recent examples include fires in tunnels: Channel (1996), Mont-Blanc and Tauern (1999), Kaprun (2000) and Saint-Gothard (2001). In the USA, the World Trade Center attack, is another tragic example.

It is important to assess materials changes caused by high temperatures.[1–3] In the present study, we measured room-temperature elastic modulus (E^*) of Portland cement pastes, mortars, and 'microconcretes' that had been subjected to cumulative thermal treatments at temperatures up to 1000°C. E^* was measured by a non-destructive ultrasonic technique at a frequency of 10 MHz. Elastic moduli experiments were complemented by mercury intrusion porosimetry, scanning electron microscopy, X-ray diffraction, and thermal analysis.

Elastic moduli are of interest for three different reasons.

(*a*) Knowledge of elastic moduli is required to establish the stress–strain relationship within a loaded structure, for instance when using finite-elements methods.

(*b*) Elastic properties are 'intrinsic properties' of materials, since elastic constant are second-order derivatives of cohesion forces in relation to displacements.[4] In contrast, strength and fracture-related parameters are 'extrinsic properties', which are mainly controlled by microstructural defects.[5,6] For low-ductility materials, the scattering of experimental data is much lower for intrinsic properties than for extrinsic.[7]

(*c*) Elastic moduli can be measured using non-destructive methods, which allow the effect of cumulative treatments to be determined.

Experimental

Materials

Table 1 gives information on the eight materials we studied, namely three pastes, three mortars and two microconcretes. The cement was a Portland composition (Tables 2 and 3) with Blaine surface area of 3820 $cm^2 \times g^{-1}$. The mortar aggregate was siliceous sand (98·6% α-quartz, 100–630 μm grain size, 3% total porosity) or calcareous sand ($CaCO_3$ with a small content of quartz, 80–800 μm grain size, 12% total porosity). The microconcrete was made with cement,

* Ecole Supérieure de Physique et de Chimie Industrielles, F-75231 Paris Cedex 05.

† Association Technique de l'Industrie des Liants Hydrauliques, F-92974 Paris-La Défense.

Table 1. Materials

Material	Paste	Paste	Paste	Mortar	Mortar	Mortar	Concrete	Concrete
Sand nature	—	—	—	siliceous	siliceous	calcareous	siliceous	siliceous
Silica fume	—	—	—	—	—	—	SF	SF
Binder*:sand				0·33	0·33	0·33	0·33	0·33
Water:binder	0·25	0·35	0·5	0·35	0·5	0·5	0·25	0·35
Superplast.**	—	—	—	SP	SP	SP	SP	SP
Label	2NP	3NP	5NP	3NS	5NS	5NC	2OS	30S

Notes:
* 'Binder' is cement for paste and mortar and cement plus 15% of silica fume for concrete.
** 2% by cement wt. of polycarbonxylate superplasticizer were added to mortar and concrete.

Table 2. Chemical composition of the cement (CPA CEM I 52·5 CP2 ENV 197-1 NF-P 15-301, NF-P 15-318) (wt %)

SiO_2	Al_2O_3	Fe_2O_3	CaO	SO_3	K_2O	MgO	Na_2O	Free lime	Ignition loss
20	5·3	2·5	64	3·2	1	1	0·15	0·7	2·4

Table 3. Bogue's composition of the cement (wt %)

C_3S	C_2S	C_3A	C_4AF
61·5	10·5	10	7·5

siliceous sand, and silica fume (0·35 μm). The preparation of mortar and microconcrete was facilitated by adding a polycarboxylate superplasticiser (2% by cement weight).

Several samples were replicated to check the reproducibility of experiments. For ultrasonic measurement, three cylindrical specimens of each composition were molded in silicone molds (15 mm in diameter and 15–19 mm in height) and vibrated at 40 Hz for 10 min to facilitate degassing. The vibration treatment did not lead to segregation of components and bleed water. For porosimetry measurements and SEM, at least two specimens for each technique were made by cutting pellets (≈ 1 cm^3) from bars that had been cast and vibrated in silicone molds (10 × 10 × 80 mm). Cutting was made using a circular diamond saw sprayed with ethanol to avoid any change in the hydration degree. DTA/TG and XRD measurements were carried out on finely ground materials.

Cure and thermal treatment

After 24 h at room temperature in a closed glass vessel, saturated with water, the specimens were demolded and cured for 7 days or 28 days. Then, the specimens were submitted to cumulative thermal treatments at fixed soaking temperatures (T).

An electric oven was used for treatments at 80, 120, 150 and 200°C, whereas an electric muffle furnace was used for treatments at temperatures of 250, 300, 400, 500, 600, 700, 800 and 1000°C. In the oven, the thermal program was heating at 0·2°C × min^{-1} to T, soaking for 10 h, then natural cooling. In the furnace, the rate of heating was 3·0°C × min^{-1} to the maximum temperature reached in the previous treatment but thereafter 0·2°C × min^{-1} to new soaking temperature. Soaking was still 10 h, followed by natural cooling.

We have to point out that the purpose here was to study the changes experienced by a *material*, not to evaluate the damage suffered by a *building* or a *civil engineering structure*. To collect reproducible materials data, we have to be close to thermal equilibrium, which explains the choice of small-size specimens and of low heating rates. Studies on thermal shock behaviour of brittle materials (glass, ceramics and cementitious materials) have shown that the best approach[8] is that of decoupling the variables. Transient effects, in particular thermal gradients and, therefore, differential strains, can be studied using numerical methods (for instance 3D finite elements) which are fed with the relevant materials data. They have to be complemented by experimental studies on bulky specimens, in particular to take into account spalling[3,9] and effects of pore pressure.[10]

Elastic modulus measurement

Non-destructive dynamical methods can use either standing waves or travelling waves to measure elastic constants. The standing wave methods (resonance methods) work by exciting bars or discs to their resonance frequencies, usually in the kilohertz range. The travelling-wave methods work by measuring the time of flight of waves (longitudinal, shear or surface), usually in the megahertz range.

For resonance methods, both the *resonance frequencies* of vibrating samples and their *damping capacity* are very sensitive to the presence of accidental defects, in particular cracks, and to the location of those defects. For the present study, however, the goal was to evaluate the changes in elasticity without being too much affected by the presence of thermally-induced cracks. From this point of view, the travelling wave methods offer the advantage[11,12] that the *time of flight*

is not much affected by accidental defects, although those defects can induce *extra echoes* and increase *acoustic attenuation*.[13] We therefore chose to operate with a travelling wave method.[11,12]

The only case where the physical meaning of elastic constants is unequivocal is that of a dense, single phase, vitreous or single crystalline material. In the general case of a porous, microcracked, multiphase and polycrystalline material, we can only estimate average values.[14] One requirement is that the 'microstructure scale' (that is the scale of heterogeneities such as pores, grains, microcracks or inclusions) is small in comparison with the dimensions of the sample that is used for the experiment.

Elasticity in isotropic solid is characterised by two moduli, Young's modulus, E, and shear modulus, G, and, therefore, the determination of both E and G requires two independent measurements, generally that of longitudinal wave velocity, v_l, and shear wave velocity, v_S. For acoustic waves traveling through an infinite isotropic medium[11,12]

$$E = \rho v_l^2 \frac{(1+\nu)(1-2\nu)}{(1-\nu)} \tag{1}$$

where ρ is apparent bulk density (in $\mathrm{kg} \times \mathrm{m}^{-3}$) and ν is Poisson's ratio, and

$$G = \frac{\mathrm{E}}{2(1+\nu)} \tag{2}$$

From an experimental point of view, the use of longitudinal waves is much easier than that of shear waves. It is of common practice, therefore, to limit the experiments to longitudinal waves and to consider the term ρv_l^2 (often designated E^*) instead of E

$$E^* = E/k$$

with

$$k = \frac{(1+\nu)(1-2\nu)}{(1-\nu)} \tag{3}$$

In general, the changes in E^* reflect the changes in E, since Poisson's ratio does not vary very much around a typical value of 0·27 for cementitious materials. In heat treated specimens, however, thermal damage leads to a decrease in both E and Poisson's ratio, ν.[15] Since a decrease in ν leads to an increase in k, the changes in E^* are higher (in absolute value) than the changes in E.

Ultrasonic experiments were carried out at room temperature using a Sofranel equipment. The emitter (Microscan transducer from Panametrics, 6 mm in diameter) generates short pulses at 10 MHz. One can work in echo mode (the same transducer is alternatively emitter and receiver) or in transmission mode (the emitter is on one side of the cylindrical sample and the receiver is on the other, parallel side) (Fig. 1). Acoustic coupling was insured by a gel whose high viscosity avoids intrusion into the sample porosity. Apparent bulk density, ρ, was determined by Archimedes displacement in ethanol.

The longitudinal wave velocity is deduced from the time of flight, τ, which corresponds to one travel through the specimen. In echo mode

$$\mathrm{v_l} = \frac{2L}{\tau} \tag{4}$$

For ultrasonic experiments, 'infinite medium' requires specimen dimensions, L, much larger than wavelength, λ

$$\lambda \ll L \tag{5}$$

equation (5) is verified here, since $\lambda_{10\,\mathrm{MHz}}$ is 0·2–0·4 mm, whereas L is 17 mm ± 2 mm.

The aforementioned condition that the size of heterogeneities, D_h, is small in comparison with sample dimensions is also verified, since the sand particles are below 0·6 mm.

Other characterisations

Porosity was measured using a Carlo Erba porosimeter (series 2000 WS), with mercury pressure up to 2000 bars. The pressure range we used allows the mercury to intrude pores from 3·7 nm to 7500 nm. Only open porosity can be accessed, but high pressures can break the walls of closed pores and transform then to open pores.

Powder XRD patterns were recorded using a Philips PW-1729 diffractometer in Bragg-Brentano configuration (2θ ranging from 10 to 90° by steps of $0{\cdot}02 \times \mathrm{s}^{-1}$). DTA and TG analyses were carried out using a Thermal Analyst Instruments SDT 2960 apparatus, with heating rate of $5°\mathrm{C} \times \mathrm{min}^{-1}$ from room temperature to 1000°C (air, alumina as reference). Microstructures were investigated using a JEOL JSM-5200 microscope equipped with an Oxford Instruments EDX analyser.

Results and discussion

Effects of temperature

The main events that are expected to occur in heated concrete are as follows.[16]

(*a*) From room temperature to 120–200°C, there is vaporisation of free and adsorbed water.

(*b*) Between 450–500°C, portlandite loses water to give free lime

$$Ca(OH)_2 \rightarrow CaO + H_2O$$

(*c*) In concrete with siliceous aggregate, the transformation of α-quartz to β-quartz occurs at $T = 573$°C. This transformation is accompanied by a volume expansion of ~1%, which can initiate cracking and decrease strength.[17]

(*d*) In the range 600–700°C, the reactions that follow the decomposition of various calcium silicate hydrates (for example jennite or tobermorite-like phases) can generate new phases, such as β-C_2S, as mentioned by Lin *et al.*[18] Moreover, calcium carbonate ($CaCO_3$) produced during curing release CO_2 in the range of 600–700°C: this was confirmed by TG coupled with mass spectroscopy experiments, as indicated above.

(*e*) Between 700–900°C, calcite (the main component of calcareous aggregate) decomposes to free lime

$$CaCO_3 \rightarrow CaO + CO_2$$

As far as mechanical properties are concerned, both elastic modulus[19] and fracture strength are affected.[1,2] Three domains can be distinguished.[20,21]

(*f*) From room temperature to ~400°C, high-strength concrete (HSC)[22] shows lower strength loss (1–10%) than normal-strength concrete (NSC) (15%).

(*g*) From ~400–800°C, strength loss is severe in both HSC and NSC, although HSC undergoes less degradation than NSC.

(*h*) For temperatures above ~800°C, residual strength has marginal value in both materials.

Thermal analyses

Thermal analysis data confirm the sequence of events described above. Before heat treatment, the materials were generally dried at 80°C to eliminate excess water, to avoid the cracking and spalling effects induced by fast evaporation. Fig. 2 shows the large endothermic peak observed in non-dried materials, whereas Figs 3 and 4 show the absence of such a peak in dried materials.

In pastes (2NP-28d, see Fig. 2), the DTA+TG curves show two main events, labelled as '1' (loss of free and adsorbed water, ~125°C) and '2' (dehydration of portlandite, ~450°C). Both events are associated with a weight loss. Between 650 and 700°C, there is a third event (labelled '3'), of small amplitude, also associated with a weight loss. TG coupled with mass spectroscopy experiments have shown that this effect is due to decarbonation of the carbonated species present in the material.

In siliceous microconcrete (3OS-7d, see Fig. 3), there are four events, the third one ('3') being related to the α-to-β quartz transformation at 573°C.

In calcareous mortars (5NC-28d, see Fig. 4) the decarbonation of calcite ('3') is responsible for an endothermic peak between 700 and 800°C, associated with a large weight loss.

Elastic modulus

Ultrasonic measurements show excellent reproducibility. For samples coming from a given batch (cement paste, mortar, or microconcrete), the scattering is always below 3% in either echo mode or in transmission mode. This excellent reproducibility is obtained in spite of the fact that the samples are coupled/decoupled with/from the transducers for successive experiments.

Cement pastes

In pastes cured for 7 days, the acoustic velocities (Fig. 5) are ranked according to $v_l(2NP) > v_l(3NP) > v_l(5NP)$, whatever the temperature of treatment. This confirms that E^* increases as w/c decreases; that is, as porosity decreases.

An increase in the temperature of thermal treatments results in a decrease in E^*, as mentioned in the literature.[23] Immediate loss of strength after firing is attributed to the dehydration of cement paste gel.[24] Four main domains can be distinguished.

(*a*) Near 80°C, which is the lowest temperature investigated, free water evaporates and porosity increases, which leads to a drop in E^*.

(*b*) From 80°C to a temperature T_C, E^* does not change very much. The value of T_C increases as w/c decreases. T_C is ~250°C for w/c = 0·50, ~300°C for w/c = 0·35, and ~400°C for w/c = 0·25.

(*c*) From T_C to 600°C, E^* continues to decrease. This is thought to be connected with the decomposition of portlandite, which leads to microstructural changes and gaseous emission, thus cracking and porosity.

(*d*) At temperatures above ~800°C, however, E^* regains higher values, because of presumed sintering phenomena.[18,25]

When compared with pastes cured for 7 days, pastes cured for 28 days have lower porosity and higher CSH content. This causes higher cohesion, higher strength, and higher elastic modulus (Fig. 6). As far as the

effects of thermal treatments are concerned, the main difference occurs in domain '3', where the drop in E^* as temperature increases is larger in 28 day-cured pastes than in 7 day-cured pastes. Moreover, the value of E^* after treatment at 1000°C is lower in the former materials than in the latter.

Pastes with w/c of 0·25 (2 NP series) have acoustic velocities that are 20–30% higher than those of pastes with w/c of 0·50 (5 NP series). This difference of 20–30% is lower than it was found in 7 day-cured pastes, showing that the influence of the w/c ratio is particularly marked in the initial stages of cement setting and hardening.

Mortars and microconcretes

In mortars and microconcretes cured for 7 days (not shown here), elastic modulus continuously decreases as the temperature of thermal treatment increases up to 800°C. For temperatures below 300°C, the acoustic velocity is greater in mortars than in the corresponding pastes having the same w/b and thermal treatment. For temperatures above 300°C, however, the drop in E^* is larger in mortars than in cement pastes. This is also true when comparing 3 OS-microconcretes with 3 NP-pastes, but is not valid when comparing 2 OS-microconcretes with 2 NP-pastes, because of the marked influence of the w/c ratio during the initial stages of hydration, as explained above. Finally, when the temperature of treatment is very high ($T > 800$°C), the sintering phenomena cause a large increase in acoustic velocity and elastic modulus, as observed in pastes.

The results for mortars and microconcretes cured for 28 days (Fig. 7) are qualitatively similar to those for materials cured for 7 days. As for pastes, the 28 day materials exhibit higher values of E than the 7 day corresponding materials.

Ultrasonic evaluation becomes more and more difficult as the specimens become more and more cracked; cracking increases acoustic attenuation and reduces pulse heights. For the calcareous mortars, which are the most sensitive to thermal damage, measurement becomes impossible when the temperature of treatment exceeds 600°C. For the microconcretes containing silica fume (2 OS and 3 OS), which are the most resistant to thermal damage, measurement is still possible after treatment at 1000°C. These facts could be related to the lower porosity of siliceous aggregate (3%) compared to calcareous aggregate (12%), as well as to the effect of silica fume[26–28] as a filler in microconcretes.

Figures 8 and 9 show the changes in $E^*(T)/E^*_0$ vs. T – where $E^*(T)$ is the value of E^* after treatment at temperature T and E^*_0 the value before any heat treatment. One observes that all materials in a given category exhibit same changes in $E^*(T)/E^*_0$ vs. T, whatever the w/b ratio, which suggests the existence of a 'master curve' for each category. The calcareous mortars do not confirm well to this trend however, which might be due to the porous structure of calcareous aggregate. Complementary experiments (not detailed here) have been conducted by varying the nature of cement: they have confirmed this parameter is a second-order parameter by comparison with the nature of material, i.e. a paste or a mortar/microconcrete.[29]

Porosity

Thermal treatments result in an increase in both total porosity (Fig. 10) and pore size (Fig. 11). For the highest temperatures that have been investigated, however, there is a slight decrease in total porosity: this can be attributed to sintering.[30]

Microstructure

Thermal treatments cause cracking[31] (examples are given in Figs 12–16), but sintering phenomena can allow crack healing in materials subjected to very high temperatures (1000°C). The w/c or w/b ratios have a marked influence on cracking. For cement pastes with w/c = 0·50, the 7 day-cured samples are densely cracked after treatment at 700°C whereas the 28 day-cured samples are densely cracked only after treatment at 500°C. As previously mentioned, ultrasonic measurement is not possible in badly cracked materials. For mortars, cracking becomes visible at temperatures around 300°C, then develops during stage '3', as defined above. The calcareous mortars are more sensitive to cracking than the siliceous ones. The former are densely cracked after treatment at 500°C (7 day-cured

materials) and 600°C (28 day-cured materials), whereas the latter show modest cracking after treatment at 600°C.

Conclusion

(*a*) Room-temperature elastic modulus (E^*) of heat-treated materials decreases when the temperature of treatment increases. Four domains can be distinguished, namely: (i) room temperature to ~80°, (ii) ~80°C to T_C (where T_C increases from ~250–400°C when w/c decreases); (iii) T_C to ~600°C; and (iv) $T >$~600°C. For treatments at very high temperatures ($T > 800$°C), however, E^* can regain, which must be due to sintering.

(*b*) All materials in a given category (i.e. pastes, mortars, and microconcretes) exhibit same changes in $E^*(T)/E^*_0$ vs. T, whatever the w/b ratio, which suggests the existence of a 'master curve' for each category.

(*c*) Porosity and pore size increase as temperature increases up to 700°C. At higher temperatures, sintering yields densification.

(*d*) The aim of the study was to collect materials data from small specimens close to thermal equilibrium. This means that the results cannot be directly extrapolated to bulk parts, where one has to take into account temperature gradients, heterogeneities, migration of water vapor,[5] and mechanical constraints due to metallic reinforcement. Another comment is that repetitive thermal cycling can lead to stress accumulation in siliceous concrete, due to the $\alpha \leftrightarrow \beta$ quartz inversion, which means the present study (one-time-only cycling) must not be extrapolated to repetitive thermal cycling. Finally, one must recall that much damage occurs in fire situations where free lime is formed (temperatures $>$ 600–800°C). Upon rewetting, explosive spallation may disintegrate the concrete. Those comments must be made to avoid the conclusions of the present study will be taken out of context.

Acknowledgements

The study was supported by Association Technique de l'Industrie des Liants Hydrauliques (ATILH). The authors are very grateful to Jérôme Latournerie and Djamila Hourlier (SPCTS Laboratory, University of Limoges) for the TG-MS experiments.

References

1. ULM F.-J., COUSSY O. and BAZANT Z. P. The 'Chunnel' Fire. I: Chemoplastic softening in rapidly heated concrete. *Journal of Engineering Mechanics*, 1999, March, 272–282.
2. ULM F.-J., ACKER P. and LEVY M. The 'Chunnel' Fire. II: Analysis of concrete Damage. *Journal of Engineering Mechanics*, 1999, March, 283–289.
3. SANJAYAN G. and STOCKS L.J. Spalling of high-strength silica fume concrete in fire. *ACI Materials Journal*, 1993, **90**, No. 2, 170–173.
4. NYE J. F. *Physical properties of crystals. Their representation by tensors and matrices*, Oxford Science Publications, Oxford, 1985.
5. WACHTMAN J. B. *Mechanical properties of ceramics*, John Wiley & Sons, New York, 1996.
6. LAWN B. *Fracture of brittle solids*, Cambridge Solid State Science Series (E. A. Davis and I. M. Ward (Eds)), 1993.
7. MORRELL R. *Handbook of properties of technical and engineering ceramics. Part I – An introduction for the engineer and designer*, National Physical Laboratory, London: Her Majesty's stationery office, 1985.
8. HASSELMAN D. P. H. Thermal Stress Resistance of Engineering Ceramics. *Materials Science and Engineering*, 1985, **71**, 251–264.
9. SARVARANTA L. and MIKKOLA E. Fiber mortar composites under fire conditions: effects of ageing and moisture content specimens. *Materials and Structures*, 1994,. **27**, 532–538.
10. KALIFA P., MENNETEAU F.-D. and QUENARD D. Spalling and pore pressure in HPC at high temperatures. *Cement and Concrete Research*, 2000, **30**, 1915–1927.
11. ROYER D. and DIEULESAINT E. *Elastic waves in solids. Part I – Free and guided propagation*, Springer, Heidelberg, 2000.
12. ROYER D. and DIEULESAINT E. *Elastic waves in solids. Part II – Generation, acousto-optic interaction, Applications*, Springer, Heidelberg, 2000.
13. MONTEIRO P. J. M. and KING M. S. Experimental studies of elastic wave propagation in high-strength mortar. *Cement, Concrete and Aggregates*, 1988, **10**, No. 2, 68–74.
14. HASHIN Z. and SHTRICKMAN S. A variational approach to the theory of elastic behavior of multiphase materials. *Journal of the Mechanics and Physics of Solids*, 1963, **11**, 127–140.
15. MARECHAL J.-C. Variations in the modulus of elasticity and Poisson's ratio with temperature. *Concrete for Nuclear Reactors*, 1970, ACI SP 34-27, 495–503.
16. FERAILLE-FRESNET A. *Le rôle de l'eau dans le comportement à haute température des bétons*. PhD, thesis, Ecole Nationale des Ponts et Chaussées, Paris, 2000.
17. ABRAMS M. S. *Compressive strength of concrete at temperatures to 1600F. Effect of temperature on concrete*, 1973, ACI SP 25-2, 33–58.
18. LIN W.-M., LIN T. D. and POWERS-COUCHE L. J. Microstructures of fire-damaged concrete. *ACI Materials Journal*, 1996, May–June, 199–205.
19. NASSIF A. Y., RIGDEN S. and BURLEY E. The effects of rapid cooling by water quenching of the stiffness properties of fire-damaged concrete. *Magazine of Concrete Research*, 1999, **51**, 255–261.
20. CHAN Y. N., PENG G. F. and ANSON M. Residual strength and pore structure of high strength concrete and normal strength concrete after exposure to high temperatures. *Cement and Concrete Composites*, 1999, **21**, 23–27.
21. CHAN Y. N., LUO X. and SUN W. Compressive strength and pore structure of high-performance concrete after exposure to high temperature up to 800°C. *Cement and Concrete Research*, 2000, **30**, 247–251.
22. JAHREN P. A. Fire resistance of high strength/dense concrete with particular reference to the use of condensed silica-fume – A review. *Proceedings of the 3rd International Conference on Fly Ash, Silica Fume, Slag & Natural Pozzolans in Concrete, Trondheim.* ACI SP 114-50, Detroit, USA, 1989, pp. 1013–1049.
23. CRUZ C. R. Elastic properties of concrete at high temperatures. *Journal of the Portland Cement Association Research and Development Laboratories*, Skokie, IL, 1966, **1**, 37–45.

24. CROOK D. N. and MURRAY M. J. Regain of strength after firing of concrete. *Magazine of Concrete Research*, 1970, **22**, 149–154.
25. ROSTASY F. S., WEISS R. and WIEDEMANN G. Changes of pore structure of cement mortars due to temperature. *Cement and Concrete Research*, 1980, **10**, 157–164.
26. HEKAL E. E. Effect of silica fume on physicochemical and mechanical properties of hardened cement pastes: I – hydration kinetics, phase composition and compressive strength. *Sil Ind, 2000*, **64**, Nos 9–10, 163–167.
27. HEKAL E. E. Effect of silica fume on physicochemical and mechanical properties of hardened cement pastes: II – dehydration-rehydration of the hardened cement pastes. *Silicates Industriels*, 2000, **65**, Nos 1–2, 9–18.
28. HEKAL E. E. Effect of silica fume on physicochemical and mechanical properties of hardened cement pastes: I – hydration kinetics and microstructure of hydrates. *Proceedings of the 19th International Conference on Cement Microscopy, Cincinnati, Ohio, USA*, 1997, 103–117.
29. MASSE S., VETTER G. and BOCH P. Non-destructive ultrasonic evaluation of thermal damage in cementitious materials. *7th Conference and Exhibition of the European Ceramic Society*, Brugge, *Key Engineering Materials*, Trans Tech Publications Ltd, Zurich, in press.
30. PIASTA J., SAWICZ Z. and RUDZINSKI L. Changes in the structure of hardened cement paste due to high temperature. *Matériaux et Constructions (Paris)*, 1984, **17**, No. 100, 291–295.
31. PIASTA J. Heat deformation of cement paste phases and the microstructure of cement pastes. *Matériaux et Constructions (Paris)*, 1984, **17**, No. 102, 415–420.

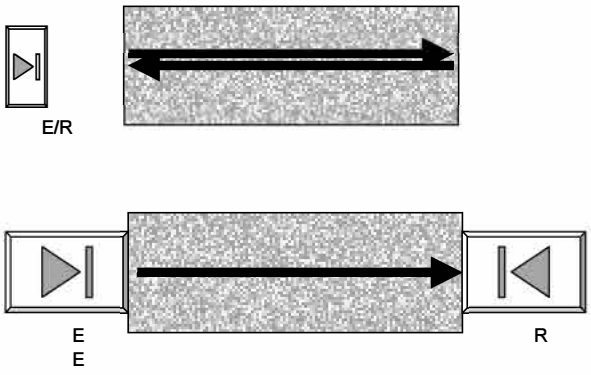

Fig. 1. Ultrasonic methods. E is the emitter and R the receiver. Echo mode (top) and tramission mode (bottom)

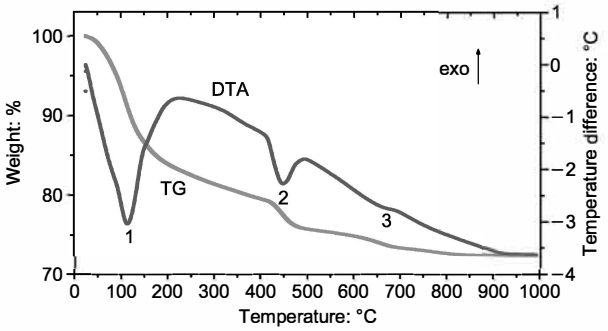

Fig. 2. DTA/TG of material 2NP28 000 (paste, $E/C = 0{\cdot}25$, cure = 28 days)

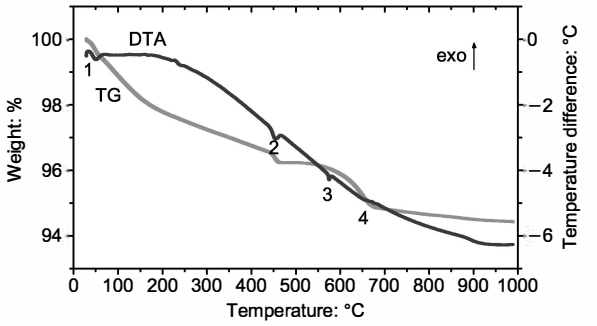

Fig. 3. DTA/TG of material 3OS7 080 (microconcrete with siliceous sand and fume silica, $E/C = 0{\cdot}35$, cure = 7 days)

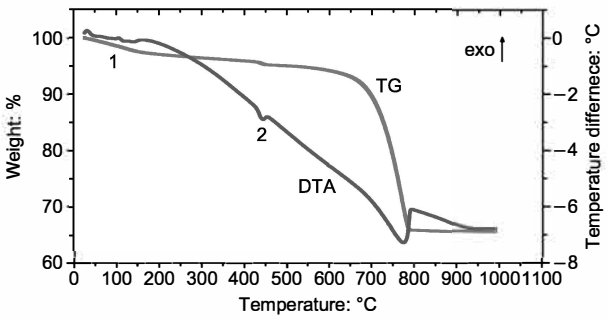

Fig. 4. DTA/TG of material 5NC28 080 (mortar with calcareous sand, $E/C = 3{\cdot}50$, cure = 28 days)

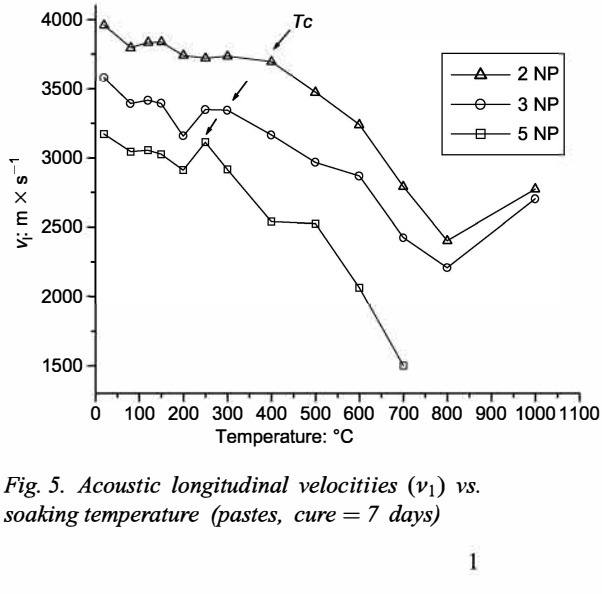

Fig. 5. Acoustic longitudinal velocitiies (v_1) vs. soaking temperature (pastes, cure = 7 days)

1

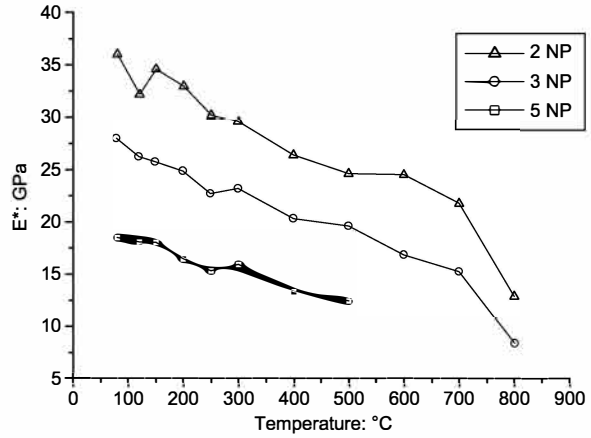

Fig. 6. Room-temperature elastic modulus (E^*) vs. soaking temperature (pastes, cure = 28 days)

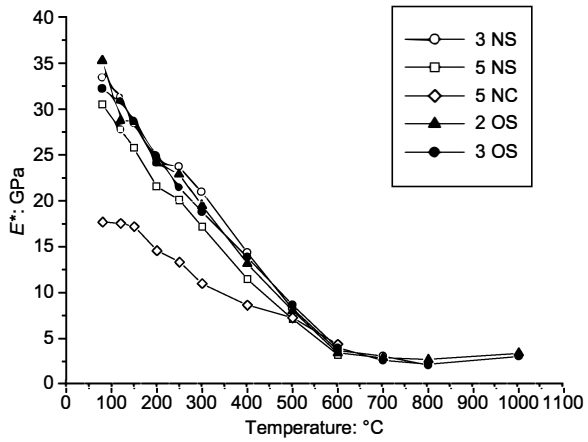

Fig. 7. Room-temperature elastic modulus (E^*) vs. soaking temperature (mortars and microconcretes, cure = 28 days)

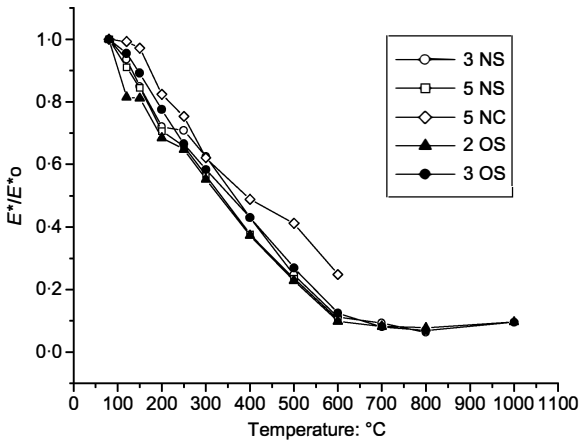

Fig. 9. E^*/E_0^* vs. soaking tempeature (E_0^* is initial elastic modulus), (mortars and microconcretes, cure = 28 days)

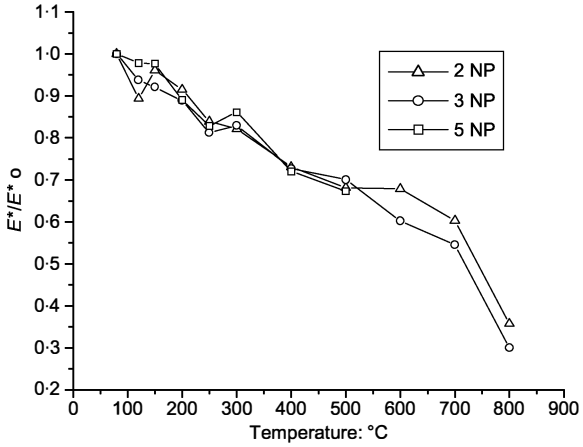

Fig. 8. E^*/E_0^* vs. soaking temperature (E_0^* is initial elastic modulus), (pastes, cure = 28 days)

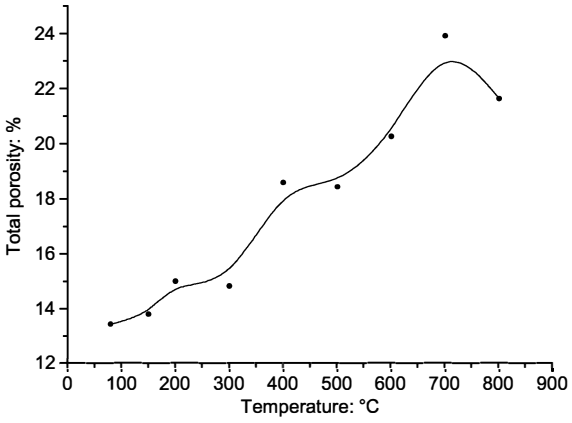

Fig. 10. Siliceous microconcrete: total porosity vs. soaking temperature

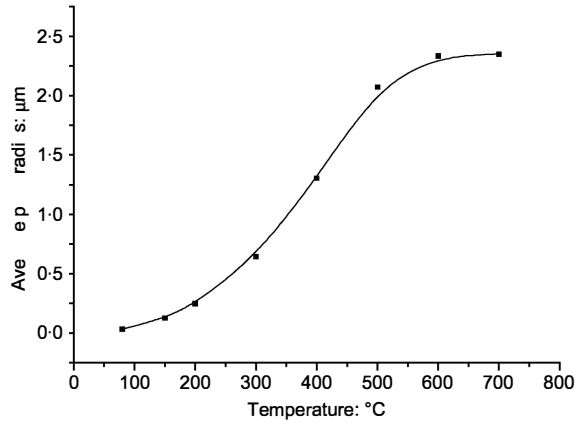

Fig. 11. Siliceous microconcrete: mean pore size vs. soaking temperature

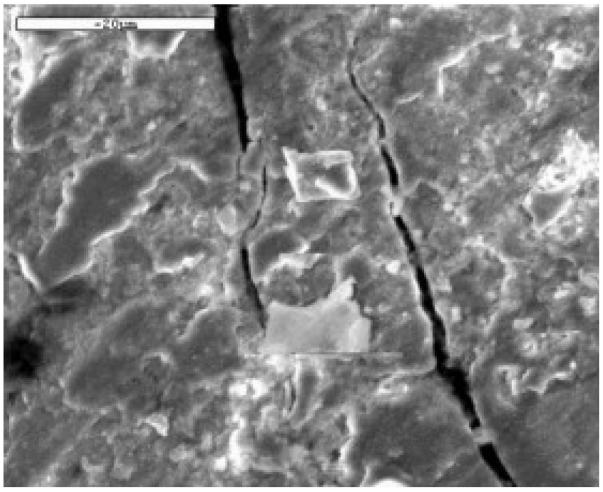

Fig. 12. Cracking after soaking at 400°C: paste, $E/C = 0{\cdot}25$, cure = 7 days

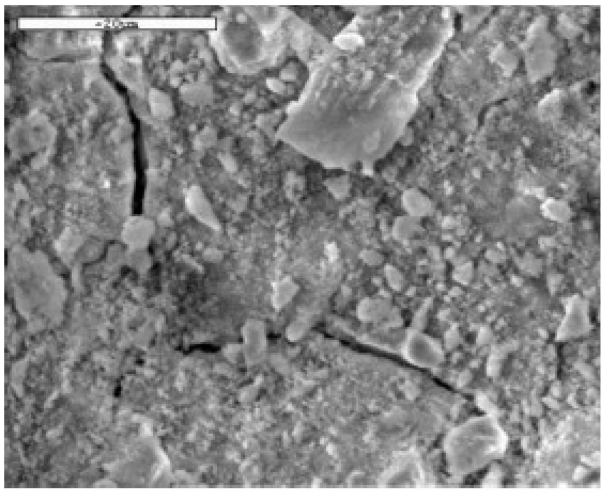

Fig. 13. Cracking after soaking at 700°C: paste, $E/C = 0{\cdot}25$, cure = 7 days

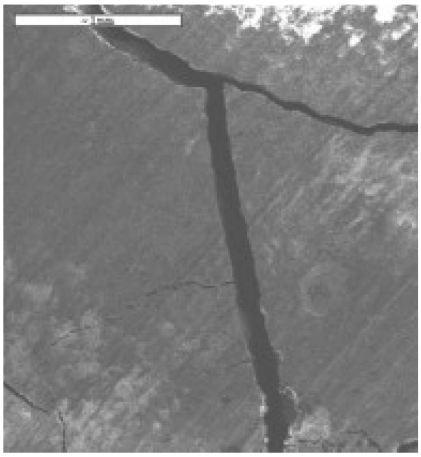

Fig. 14. Soaked at 600°C: paste, $E/C = 0{\cdot}50$, cure = 7 days

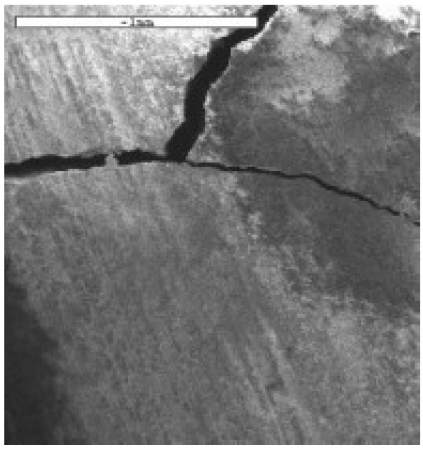

Fig. 15. Soaked at 800°C: paste, $E/C = 0{\cdot}50$, cure = 7 days

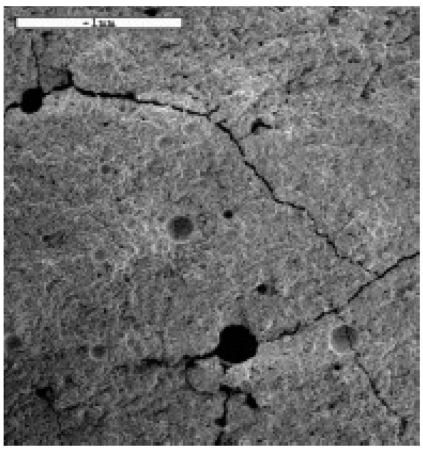

Fig. 16. Soaked at 1000°C: paste, $E/C = 0{\cdot}50$, cure = 7 days